# Second Harmonic 210 GHz InP Millimeter Wave Transferred Electron Oscillators

*M.F. Zybura, S.H. Jones, G.B. Tait*[†]

Applied Electrophysics Laboratories
Department of Electrical Engineering
University of Virginia
Charlottesville, VA 22903-2442

[†]Electronics Science and Technology Division
Naval Research Laboratory
Washington, DC 20375

## Abstract

Accurate and efficient calculations of the large-signal AC behavior of second- and third-harmonic InP Transferred Electron Oscillators (TEOs) are presented. This is accomplished by combining a novel harmonic balance circuit analysis technique with a hydrodynamic device simulator employing the temperature dependent drift and diffusion equations. The electron transport simulations include a detailed heat flow analysis to update the temperature profile in the device. The nonlinear circuit analysis utilizes a fixed-point iterative method derived from the robust multiple reflection algorithm. To expedite the process and aid in convergence, an acceleration technique is also employed in this algorithm. The associated reduction in computation time allows for the inclusion of a full hydrodynamic treatment of the Transferred

Electron Device (TED) using the first two moments of the Boltzmann transport equation. Comparisons are made with the published experimental data reported by Rydberg on second- and third-harmonic 200-300 GHz InP TEOs. Simulation results for TEOs designed specifically for 210 GHz second harmonic, and 315 GHz third harmonic are presented.

# 1 Introduction

Rydberg [1] has demonstrated as much as 0.6 mW of power at 270 GHz using third-harmonic InP devices. To optimize future harmonic device designs for increased power and higher frequencies, a design tool that efficiently determines power at all harmonics, as a function of the device characteristics, embedding circuit, and packaging parameters is required. Presently, computer aided design programs are available for microwave nonlinear circuit analysis based on the harmonic balance numerical technique [2]. These codes reduce the nonlinear semiconductor devices to equivalent circuit elements with closed form analytical approximations for the current-voltage characteristics making the nonlinear circuit analysis possible. This approach is powerful for lower frequency design, and has been a critical factor in the design of integrated microwave circuits. For more complex and higher fre-

quency millimeter wave circuits however, the approximate equivalent circuit technique is not sufficiently accurate. In this work, an efficient fixed point iteration method derived from the multiple reflection technique [2] is employed facilitating the use of a full hydrodynamic device simulator using the drift and diffusion equations. The drift and diffusion equations utilize both field (0.1-100 kV/cm) and temperature (300-500K) dependent mobility and diffusivity derived from monte carlo simulations, and a thermal analysis which includes all regions of the device. Every aspect of the linked nonlinear circuit/ hydrodynamic device simulator has been designed for accuracy, computational speed, and robust convergence properties.

## 2    Thermal Model

Since the dc-microwave conversion efficiency in TEDs can degrade substantially if the device active-region temperature approaches 500K, temperature effects must be considered to optimize high power oscillator design. During operation, heat is generated in all regions of the device, however most of the power dissipation occurs across the device active-region due to both its relatively high resistivity and low dc-rf conversion efficiency. Given the extremely low thermal conductivity of the air surrounding the mesa, es-

sentially all the heat generated in the packaged device will flow into the highly conductive gold plated copper heat sink through the device layers and contacting regions. Thus, the thermal analysis can be reduced to one dimension, with no heat loss through the sides or top of the mesa. In our model, heat generation is considered in all layers of the packaged device [3]. Integrating the associated one dimensional heat equation, and solving the resultant set of linear equations yields an expression for the temperature across a given layer as a function of the interface temperatures that bound that region. The continuity criterion is applied at every interface giving a system of linear equations with a tri-diagonal matrix for the determination of the unknown interface temperatures. To complete the mathematical description, specifications of boundary conditions at both the mesa to air, and contact to heat sink interfaces are required. At the heat sink interface the flow of heat from the semiconductor into the stud can be approximated as heat transfer into an infinite half plane. At the top of the mesa, as mentioned, it is assumed that there is no heat flow ($\frac{\partial T}{\partial x} = 0$). The symbolic solution to these equations gives closed form expressions for T and $\partial T / \partial x$ in each layer given the layer dimensions, the ohmic contact resistance, and the power dissipated per unit volume (Q) in that layer. As described below, Q is calculated in all layers from the large signal ac numerical calculation of

the device current and power.

## 3  Device Simulator

The device simulator employed here is a slightly modified version of a previously described simulation program [3, 4]. The phenomenological hydrodynamic equations governing the physical model are the reduced, one dimensional forms of the first two moments of the Boltzman Transport Equation (BTE) and Poisson's equation,

$$\frac{\partial n}{\partial t} = \frac{1}{q}\frac{\partial J}{\partial x} \tag{1}$$

$$J = qnE\mu(E,T) + qD(E,T)\frac{\partial n}{\partial x} + qnD_n^T\frac{\partial T}{\partial x}, \tag{2}$$

and

$$\frac{\partial^2 \phi}{\partial x^2} = -\frac{q}{\epsilon}(N_D(x) - n), \tag{3}$$

where n, q, and J are the electric charge density, the electron charge, and the particle current density, respectively. In equation 2, E, $\mu$, D, $D_n^T$, and T are the electric field, the temperature and field dependent mobility and diffusivity, the thermal diffusivity, and the lattice temperature, respectively. In equation 3, $\phi$ is the scaler potential, $\epsilon$ is the dielectric permittivity of the device material, and $N_D(x)$ is the donor impurity concentration. The

electric field is calculated from Poisson's equation, and the thermal gradient,

$\partial T / \partial x$, is analytically determined from the aforementioned thermal analysis.

The GaAs and InP electric field and temperature dependent mobility,

$\mu(E, T)$, and diffusivity, D(E,T), were calculated from over 300 three-valley

monte carlo simulations. These simulations were performed using 10,000

superparticles at 50 degree increments from 300K to 500K with a uniform

donor concentration of $10^{16} cm^{-3}$. The monte carlo code is similar to the

code used in [5], however to account for high temperature effects, along

with lattice temperature, several material parameters were modified to be

temperature dependent [6, 7]. These include: the energy gaps and conduc-

tion valley minima separation of $\Gamma$, L, and X valleys, the gamma valley

electron effective mass, the density and lattice constant, and the high and

low frequency dielectric constants. Both the mobility and diffusivity data

has been numerically fit using equation (6-2-8) of reference [8], and the ac-

companying fit parameters aré again fit versus temperature yielding surface

contours for both mobility and diffusivity versus electric field and temper-

ature. Closed form expressions for $\mu(E, T)$ and D(E,T) serve to enhance

computation speed. The above drift and diffusion transport equations form

a set of coupled nonlinear partial differential equations, which are solved by

the half-implicit Crank Nicolson finite difference scheme. Spatial and tem-

poral increments typically are on the order of the length and time over which charge imbalances grow or decay. Spatially, the Debye length is suitable, and temporally, the dielectric relaxation time is appropriate. This technique offers substantial reductions in CPU time while retaining some important hot electron effects since $\mu(E,T)$ and $D(E,T)$ have been extracted from prior monte carlo analysis. The frequency dependent parasitic resistances of the device (DC-$n^{th}$ harmonic) are also calculated [9] and added to the respective embedding impedances also included in the nonlinear circuit analysis described below.

## 4    Harmonic Balance

To fully design transferred electron oscillators (TEOs) equal design consideration must be given to both the device and the circuit in which it is mounted. With a hydrodynamic device simulator, one can determine the optimal embedding impedances of the cavity presented to the device by optimizing the power generation as a function of the ac voltage. However, such an optimization is virtually impossible when considering higher harmonic components of the driving voltage. Similarly, finding a device design which has some pre-specified operating impedance is difficult, when considering second- or

third-harmonic operation. By linking both the device and circuit simulators this problem can be overcome. The harmonic balance nonlinear circuit analysis technique employed here is an extension of the Siegel and Kerr multiple reflection algorithm [2]. A fixed-point iteration is used to update the total voltage at the device terminals. The current through the device then is numerically calculated as described above. In our algorithm, we use *a priori* knowledge of the solution from Kirchhoff's voltage law that the nonlinear device impedance will equal the negative of the linear circuit impedance for each undriven harmonic in steady state ($Z_n^{NL} = -Z_n^L, n = 2, 3, ..., 6$). This eliminates the computationally intensive and possibly unstable Runge-Kutta numerical integration necessary in the multiple-reflection technique, and automatically calculates the complex under-relaxation parameters for each harmonic component of the fixed point update equation. Included with the fixed-point iteration is a Steffenson acceleration scheme adopted from the secant methods of numerical analysis [10]. Unlike Newton techniques, the difficult and time consuming numerical calculations needed for the assembly of Jacobian matrices and the solutions of large linear systems of equations are avoided, while maintaining a convergence rate nearly that of Newton-type methods.

# 5  Results and Discussion

Figure 1 illustrates the algorithm by which the TEO simulations are performed. The operating frequency, DC bias, circuit embedding impedances ($2^{nd}$ – $6^{th}$ harmonic), doping profile, and chip characteristics are adjustable inputs. The ac driving voltage, $V_1$, is allowed to sweep over a given range where optimal power, stability, and sufficient device impedances at the fundamental are anticipated. This limits the optimization to the DC and fundamental driving voltages. After each fixed-point iterative update of the voltage, the device current is numerically calculated, and the circuit and device impedances at each harmonic are tested for convergence ($Z_n^{dev} = -Z_n^{ckt}, n = 2, 3, ..., 6$). Outputs include current and voltage waveforms, electric field and electron concentration profiles versus time and position, the temperature profile and output power (DC-$6^{th}$ harmonic). In order to demonstrate the correlation between simulation and experimental results, comparisons have been made with published experimental data of Rydberg [1]. The InP TED simulated and described in reference [1] has a 1.1$\mu$m graded active region from $1.4x10^{16}$cm$^{-3}$ at the cathode to $1.6x10^{16}$cm$^{-3}$ at the anode, and a 50$\mu$m mesa diameter. At a fundamental frequency of 94 GHz and DC bias of 4-V, the simulations indicate peak power and stability for an impressed

2-V ac signal directly across the device. This gives a device impedance at the fundamental of $Z_1^{dev} = -0.8 - j6.6\Omega$. Figure 2 shows the resultant power versus circuit impedance surface contour for a domain of second harmonic (188 GHz) circuit impedances ranging from $1.55\Omega \leq R_2 \leq 10.55\Omega$ and $0\Omega \leq X_2 \leq 10.0\Omega$. Because the device is typically capacitive, only positive reactances are considered. Six harmonics are considered and in this case the embedding impedances of the higher harmonics ($3^{rd} - 6^{th}$) are set to $0.001\Omega$ for both resistive and reactive components. The frequency dependent parasitic resistances are added to the corresponding linear embedding impedances. Peak performance of 6.4 mW is predicted for a second harmonic circuit impedance, $Z_2^{ckt} \approx 2.3 + j3.0\Omega$. Power generation near 2 mW is expected for circuit impedances as large as $Z_2^{ckt} = 10 + j10$. Experimentally, Rydberg has demonstrated $\approx 5$ mW of power generated at 188 GHz in second-harmonic operation.

To simulate third harmonic performance, the stable second harmonic operating impedance $Z_2^{ckt} = 2.0 + j3.5\Omega$ is selected. The third harmonic (282 GHz) power versus corresponding third harmonic circuit impedances is shown in Figure 3. Again optimal performance is predicted for a low circuit impedance, $Z_3^{ckt} \approx 2.4 + j2.0\Omega$. The anticipated output power varies from $\approx .1 - 0.76$ mW over the selected range of third harmonic circuit

impedances. At 280 GHz rydberg has shown 0.2 mW of output power. Electron concentration profiles for this device operating in third-harmonic mode with $Z_1^{ckt} = 0.8 + j6.6$, $Z_2^{ckt} = 2.0 + j3.5\Omega$, and $Z_3^{ckt} = 2.0 + j2.5$ are shown in Figure 4. The active region is bordered by regions of higher doping ($N_D = 8x10^{16}\text{cm}^{-3}$) to mimic the $n^+$ regions which bind it. Snapshots of the electron concentration are given in increments of one fifth of the fundamental frequency period. It is apparent that the device operates in an accumulation mode with the charge instabilities nucleating $\approx 0.5\mu$m from the cathode. Figure 5 show the 210 GHz second harmonic power versus the resistive part of the circuit impedance for a 2.1$\mu$m long InP TED. The device doping slopes from $1.5x10^{16}\text{cm}^{-3}$ at the cathode to $2.0x10^{16}\text{cm}^{-3}$ at the anode. The DC is 5.24 V and the magnitude of the fundamental voltage is 3.41 V. Unlike the typically short devices used for high frequency applications, this longer device produces more second harmonic power (11 mW) and has its maximum output at a larger second harmonic circuit impedance of $5.5+j10\Omega$. Figure 6 shows the resultant third harmonic (315 GHz) power from an InP Modulated Impurity Concentration TED (MICTED). The active region is 2.125$\mu$m in length with a 900$\mathring{\text{A}}$ doping mesa located 0.5$\mu$m from the cathode. The mesa is doped to $4x10^{16}\text{cm}^{-3}$ on an otherwise smooth grade from $1.5x10^{16}\text{cm}^{-3}$ at the cathode to $2.0x10^{16}\text{cm}^{-3}$ at the anode. At a fundamental frequency of

105 GHz with $V_{DC}$=5.24 V, $V_{ac}$ = 4.5 V, $Z_2^{ckt}$ = 6.45 + $j$18.0$\Omega$, and a mesa

diameter of 30$\mu$m, it is anticipated that nearly 3 mW may be obtained at 315

GHz with a third harmonic circuit embedding impedance of $Z_3^{ckt} \approx 8 + j12$.

# 6  Conclusion

The interaction between device and circuit is critical to high frequency TED

performance. With this CAD tool, efficient design of second- and third-

harmonic TEDs is possible. Typical convergence time for a given operating

point involves about ten harmonic balance iterations and a total wall time

of under a minute on a Hewlett Packard 735 workstation. Although specific

circuit embedding impedances are unavailable for Rydberg's cavity, over

the range of impedances offered, simulations compare favorably for both

second- and third-harmonic performance. The potential increase in output

power for 200-300 GHz second harmonic InP TEDs is expected for longer,

higher impedance devices. Also, increases in third-harmonic power using a

modulated doping profile in the TED active region [11] are expected and

are being further explored.

# 7   Acknowledgements

# References

[1] A. Rydberg, "High efficiency and output power from second- and third-harmonic millimeter wave InP-TED oscillators at frequencies above 170 GHz", *IEEE Electron Device Lett.*, **11**, 10 (1990), pp. 439-441.

[2] A. R. Kerr, "A Technique for Determining the Local Oscillator Waveforms in a Microwave Mixer", *IEEE Trans. Microwave Theory and Tech.* **23** (1975), pp. 828-831.

[3] M. F. Zybura, S. H. Jones, G. B. Tait and J. M. Duva, "Efficient CAD of GaAs and InP millimeter wave transferred electron devices including detailed thermal analysis", submitted *Solid-St. Electron.* 1994.

[4] G. B. Tait and C. M. Krowne, "Efficient transferred electron device simulation method for microwave and millimeter wave CAD applications", *Solid-St. Electron.* **30**, 10 (1987), pp. 1025-1036.

[5] G. U. Jensen, B. Lund, T. A. Fjeldly and M. Shur, "Monte Carlo simulation of semiconductor devices", *Comp. Phys. Comm.* **6** (1991), pp. 1-61.

[6] J. S. Blakemore, "Semiconducting and other major properties of GaAs", *J. Appl. Phys.* **53** (1982), pp. R123-R181.

[7] O. Madelung (Ed.) *Semiconductors, Group IV Elements and III-V Compounds*, Springer-Verlag, Heidelberg, Germany, 1991.

[8] M. Shur *Physics of Semiconductor Devices*, Prentice-Hall, Englewood Cliffs, NJ, 1990.

[9] S. A. Maas *Nonlinear Microwave Circuits*, Artech House, Norwood, MA, 1988, Ch. 2, pp. 49-51.

[10] J. Ortega and W. Rheinboldt *Iterative Solution of Nonlinear Equations in Several Variables*. Academic Press, New York, 1970.

[11] S. H. Jones, G. B. Tait and M. Shur, "Modulated-impurity- concentration transferred electron devices exhibiting large harmonic frequency content", *Microwave and Opt. Tech. Let.*, Vol. 5, **8**, (1992), pp. 354-359.

# Unified Numerical Device/Harmonic-Balance Nonlinear Circuit Simulator

**Inputs:**

$f_o$, $V_{DC}$, $V_{ac1}$, $Z_{2-6}^{ckt}$, $N_D(x)$, device and chip dimensions

**Harmonic Balance Algorithm**

Update Votages

$V_2$-$V_6$

**Drift and Diffusion Simulation**

Calculate Current Waveform for at least one stable oscillation period

**Discrete Fourier Transform of I(t)** DC-6th harmonic

**Device Temperature Profile Update**

**Check for Covergence** $Z_n^{dcv} = -Z_n^{ckt}$

**Output Data**

I(t), V(t), E(x,t), n(x,t), T(x), power (DC-6th harmonic)

$V_1 = V_1 + \Delta V_1$

$V_1 = V_1$ final ?

End ◄── Yes

No

Yes

No

Figure 1: Computer algorithm for the linked nonlinear circuit-hydrodynamic device simulator.

## Simulated 2$^{nd}$ harmonic Power vs. Embedding Impedance
## $f_0$=94 GHz, $V_{DC}$=4.0 V, $V_{ac}$=2.0 V
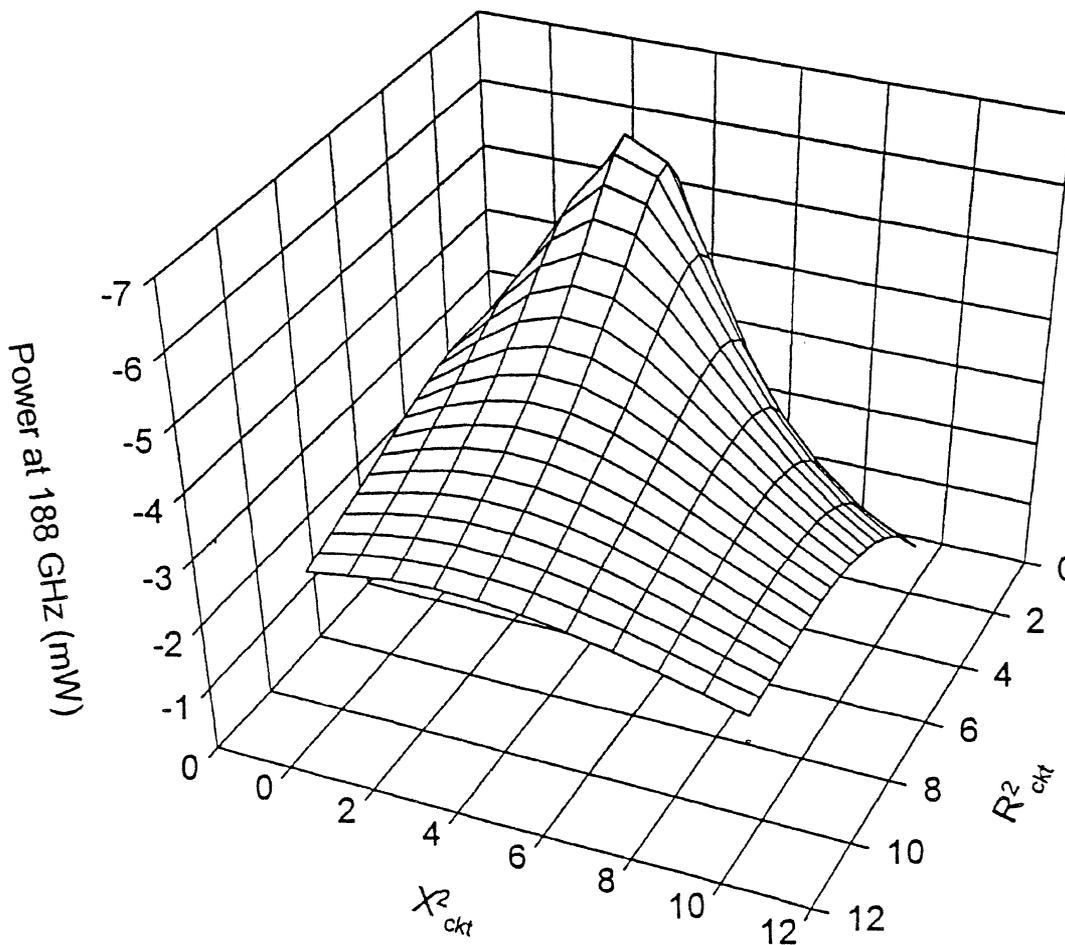


Rydberg: InP TED $I_{active}$=1.1$\mu$m, $N_D$=1.5-2.0e$^{16}$ cm$^{-3}$
Experimentally: Power at 188 GHz=5 mW

Figure 2: Second harmonic (188 GHz) power versus second harmonic circuit impedances for the device of reference [1] with $V_{DC}$ = 4.0V, $V_{ac}$ = 2.0V and $Z_1^{ckt}$ = 0.8 + $j$6.6$\Omega$. Higher harmonic ($n \geq 3$) resistive and reactive components are set to 0.001$\Omega$.

# Simulated 3rd harmonic Power vs. Embedding Impedance

## $f_0$=94 GHz, $V_{DC}$=4.0V, $V_{ac}$=2.0V, $Z^2_{ckt}$=2.0+j3.5$\Omega$
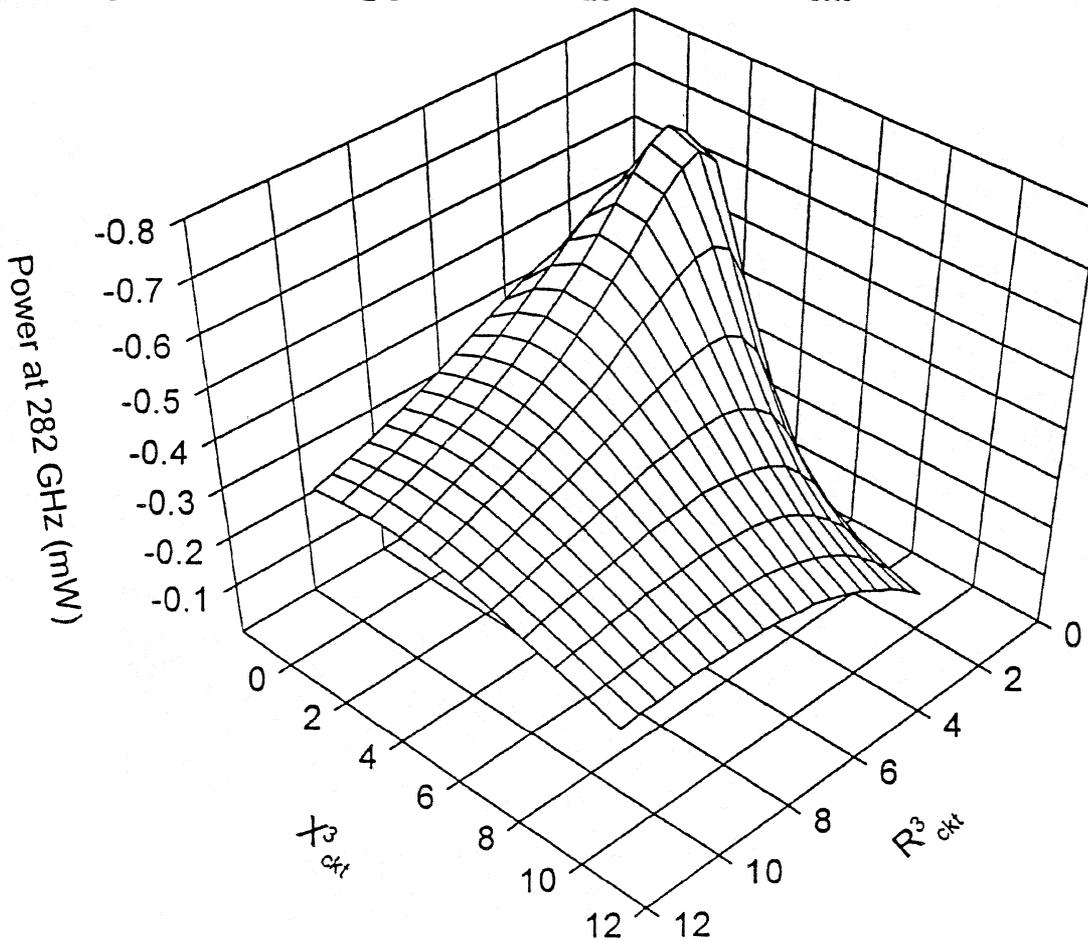


# Rydberg: InP TED $I_{active}$=1.1$\mu$m, $N_D$=1.5-2.0e$^{16}$ cm$^{-3}$
# Experimentally: Power at 282 GHz=0.2 mW

Figure 3: Third harmonic (282 GHz) power versus third harmonic circuit impedances for the device of reference [1] with $Z^{ckt}_1 = 0.8 + j6.6\Omega$, and $Z^{ckt}_2 = 2.0 + j3.5\Omega$. Higher harmonic ($n \geq 4$) resistive and reactive components are set to 0.001$\Omega$.
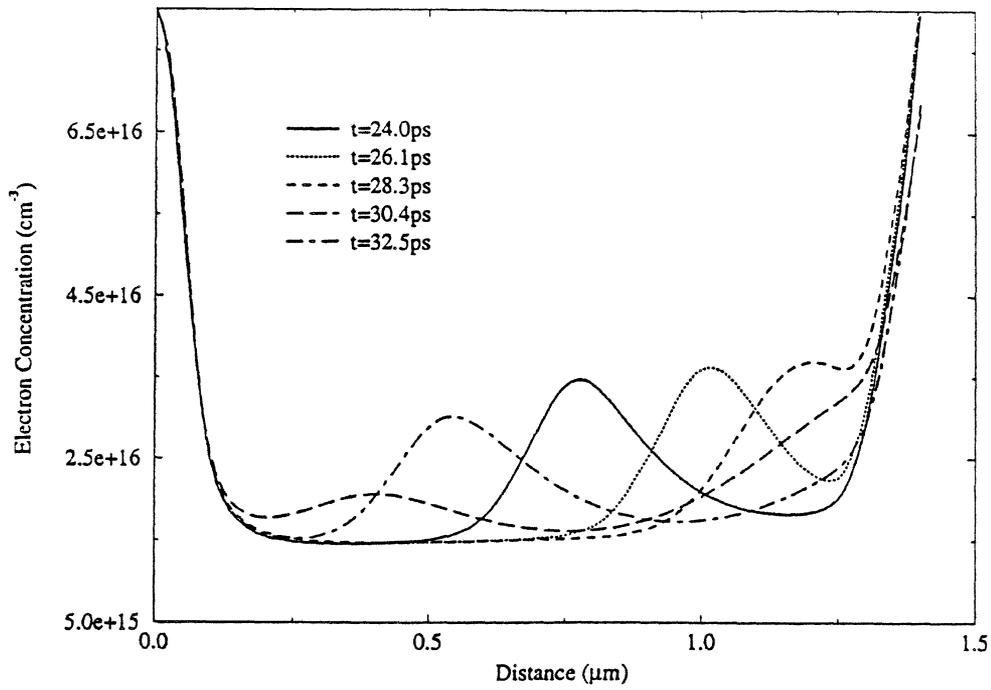
Figure 4: Simulated third harmonic (282 GHz) TED electron concentration versus time and distance for the device of reference [1]. Operating conditions are: $V_{DC} = 4.0V$, $V_{ac} = 2.0V$, $Z_3^{ckt} = 2.0+j2.5$, and a $50\mu m$ mesa diameter.
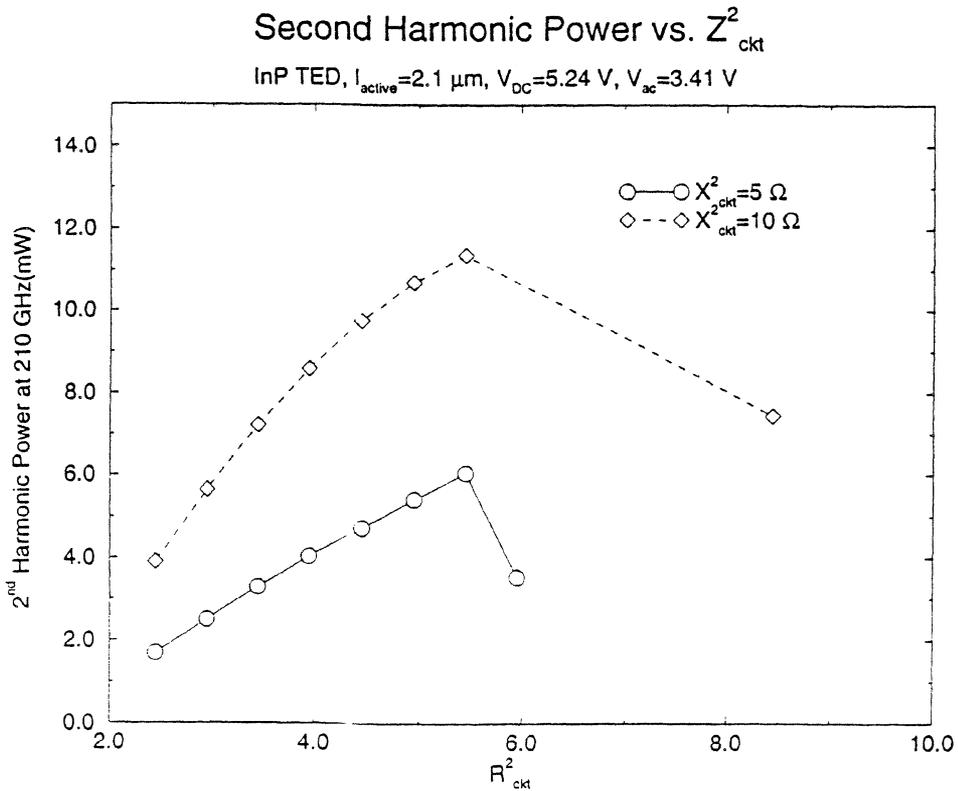


Figure 5: Simulated second harmonic (210 GHz) power versus second harmonic circuit impedances for a longer InP TED (2.1 $\mu m$). Operating conditions include $V_{DC} = 5.24$ V and $V_{ac} = 3.41$ V.

# Simulated 3rd harmonic Power vs. Embedding Impedance for InP MICTED structure, $f_0$=105 GHz
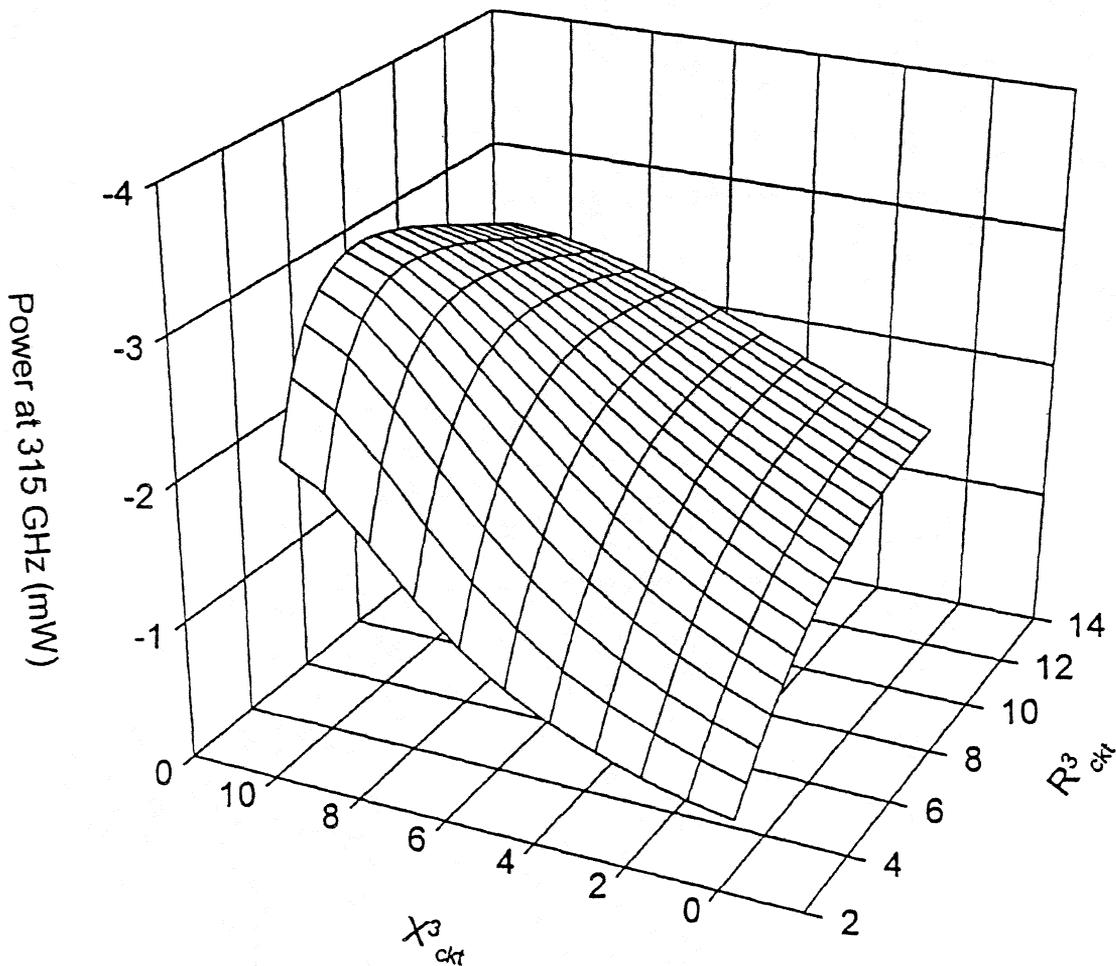


Figure 6: Simulated third harmonic (315 GHz) power versus third harmonic circuit impedances for a MICTED with $V_{DC} = 5.24$ V, $Z_1^{ckt} = 5.0 + j29.4\Omega$, and $Z_2^{ckt} = 5.45 + j18.0\Omega$. Higher harmonic ($n \geq 4$) resistive and reactive components are set to $0.001\Omega$.